Progress in Reaction Kinetics and Mechanism

ARTICLE

Open Access

https://doi.org/10.48130/prkm-0024-0001

Progress in Reaction Kinetics and Mechanism **2024**, 49: e002

Exploring fuel isomeric effects of hexanes at various pressures: pyrolysis and laminar burning velocity

Jianguo Zhang[1], Jun Fang[1], Qiying Zhang[1], Tianyou Lian[1], Songyang Li[2] and Wei Li[1*]

[1] *Institute of Aerospace Propulsion, School of Mechanical Engineering, Shanghai Jiao Tong University, Shanghai 200240, PR China*
[2] *AECC Commercial Aircraft Engine Co., Ltd, Shanghai 200241, PR China*
* Corresponding author, E-mail: lw2017@sjtu.edu.cn

Abstract

Speciation in jet-stirred reactor pyrolysis and laminar burning velocity of four hexane isomers (*n*-hexane, 3-methylpentane, 2,3-dimethylbutane, and 2-methylpentane) were measured at various pressures. The results revealed that the molecular structure of the fuel significantly influenced both the pyrolysis reactivity and the laminar burning velocities of the four hexane isomers. In the jet-stirred reactor pyrolysis, the initial decomposition temperatures of the four hexane isomers are similar, while *n*-hexane exhibits the highest laminar burning velocities, followed by 2-methylpentane and 3-methylpentane, with 2,3-dimethylbutane showing the slowest results. A comprehensive kinetic model for the four hexane isomers was proposed and subsequently validated through comparison with newly obtained experimental data. Modeling analyses were conducted to gain a deeper understanding of the fuel isomeric effects of the hexane isomers on pyrolysis characteristics and laminar flame propagation. The primary consumption pathways for the pyrolysis of four hexane isomers all involve H-abstraction reactions, followed by unimolecular decomposition. The subsequent β-scission of their primary radicals primarily governs the formation of the main products. A significant portion of 2,3-dimethylbutane is converted to propene, whereas the majority of the carbon flux from *n*-hexane is directed towards the production of ethylene. In the four hexane isomer flames, 2,3-dimethylbutane tends to produce propene and methyl radical, which have strong H-consuming ability and thus inhibit flame propagation. As a result, 2,3-dimethylbutane exhibits the slowest rate of laminar flame propagation. However, *n*-hexane tends to produce more ethyl and ethylene, which promotes flame propagation, so it demonstrates the fastest rate of laminar flame propagation.

Citation: Zhang J, Fang J, Zhang Q, Lian T, Li S, et al. 2024. Exploring fuel isomeric effects of hexanes at various pressures: pyrolysis and laminar burning velocity. *Progress in Reaction Kinetics and Mechanism* 49: e002 https://doi.org/10.48130/prkm-0024-0001

Introduction

As a crucial component of conventional transportation fuels, the combustion investigations of alkanes is of great significance for understanding the key combustion behaviors of transportation fuels, such as flame propagation, ignition, and combustion instability[1]. Alkanes are also an important component of sustainable aviation fuels, which can be used in aero engines to replace conventional jet fuel[2]. Hexane is a typical component of the alkane family. Currently, *n*-hexane has been used as a fuel additive to improve the efficiency and emission of diesel engines[3,4]. In addition, hexane is very abundant in light naphtha[5]. Figure 1 shows four hexane isomers with different molecular structures, i.e. *n*-hexane, 3-methylpentane, 2,3-dimethylbutane, and 2-methylpentane. The combustion characteristics of fuels can be significantly influenced by their isomeric structures, such as flame propagation[6–9], ignition delay time[10–12], pyrolysis reactivity[6,7,13], octane number[14], and soot generation trend[15]. Therefore, investigating the effects of fuel isomerism will enhance the understanding of how the molecular structure of fuels influences their reactivity.

Previous studies on hexane isomer combustion mainly involved the measurements of speciation information[16–21], ignition delay times (IDTs)[12,18,22–26], and laminar burning velocities (LBVs)[27–31]. It is noted that most of them focus on *n*-hexane[16–22,24,27–31], while only a few combustion studies have focused on branched hexanes[12,17,23]. Wang et al.[17] studied the low-temperature oxidation of the five hexane isomers in a jet-stirred reactor (JSR) at 1 atm, spanning a temperature range of 550 to 1,000 K. They observed that *n*-hexane exhibited the highest reactivity among the isomers, while 2,3-dimethylbutane showed the weakest reactivity at low temperatures (below 800 K). Recently, Zhang et al.[12,18] measured IDTs of five hexane isomers to examine fuel isomeric effects on ignition behavior. This was done under stoichiometric conditions at a pressure of 15 bar, using a high-pressure shock tube and a rapid compression machine, with temperatures ranging from 600 to 1,300 K. They found that the IDTs increase in the order of *n*-hexane, 3-methylpentane, 2-methylpentane, 2,2-dimethylbutane, and 2,3-dimethylbutane. To date, there are very few investigations on the pyrolysis of hexanes. Yasunaga et al.[19] studied the pyrolysis of *n*-hexane in a shock tube at 1.0–2.5 atm and 1,000–1,500 K. Some light pyrolysis products such as ethylene (C_2H_4), methane (CH_4), ethane (C_2H_6), and propene (C_3H_6) were detected and quantified by gas chromatography (GC). As is widely known, LBV is one of the crucial combustion characteristics for industrial applications in gas turbine engines and rocket propulsion systems[32], and developing chemical kinetic models[33]. Ji et al.[28] obtained the LBVs of *n*-hexane/air mixtures using counterflow configuration at the initial pressure (P_u) of 1 atm, initial temperature (T_u) = 353 K and equivalence ratio (ϕ) of 0.75–1.5. Kelley et al.[29] obtained the LBVs of *n*-hexane/air mixtures using a constant-pressure combustion chamber at P_u = 1–10 atm, T_u = 353 K, and ϕ = 0.7–1.7. Recently, Li et al.[31] obtained the LBVs of *n*-hexane/air mixtures using a high-pressure cylindrical combustion vessel at P_u = 1 atm, T_u = 353 K, and ϕ = 0.8–1.5. It can be seen that, to date, only Kelley et al.[29] measured the high-pressure LBV of *n*-hexane. There are also no previous measurements on LBVs of the other three hexane isomers and limited measurements on pyrolysis speciation information of the other three hexane isomers. In conclusion, research on the effects of fuel isomerism on laminar flame

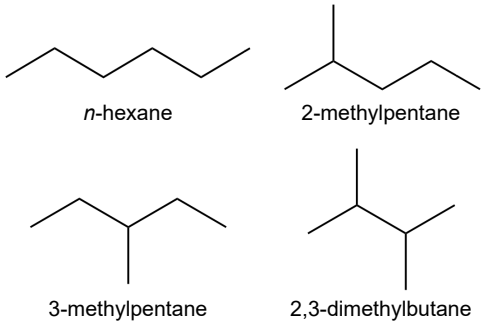

Fig. 1 Molecular structures of the four hexane isomers.

propagation and pyrolysis of the four hexane isomers remains limited.

Building on experimental advancements, kinetic models for hexane isomers have been proposed[12,18,21]. Zhang et al.[12,18] developed a comprehensive combustion reaction kinetic model of five hexane isomers (named as the Zhang model in the following study) based on IDTs and JSR oxidation species mole fraction. Recently, Belhadj et al.[21] proposed the kinetic reaction mechanism of *n*-hexane based on JSR oxidation species mole fraction. However, due to the limitations of experimental studies, the validation of basic combustion data such as LBVs and pyrolysis species mole fraction remains vague.

This work aims to explore the fuel isomeric effects of hexanes on the pyrolysis and laminar flame propagation characteristics. First, the pyrolysis of the four hexane isomers was investigated in a JSR at 1 atm using GC. Laminar flame propagation of the four hexane isomers was also investigated in a high-temperature high-pressure combustion vessel at T_u = 373 K, P_u = 1–10 atm. Second, a detailed intermediate-to-high temperature kinetic model for the four hexane isomers was developed and validated using the experimental data presented in this study and previously reported literature. Furthermore, an analysis of the fuel isomeric effects on the pyrolysis and combustion behavior of hexane isomers is performed.

Experimental methods

Jet-stirred reactor pyrolysis

The pyrolysis speciation measurements in JSR were conducted in this work. The detailed description of the quartz JSR can be found in previous work[34,35] and its design adheres to the guidelines suggested in previous studies[36,37]. Generally, the reactor features four 0.3-mm orifice nozzles positioned in the sphere with a spherical volume of 102 cm^3. During the experiments, the prepared reactant mixture was introduced into the reactor after passing through a preheating tube. The preheating tube, the spherical reactor, and the exhaust tube were all heated by adjustable heating jackets, with temperature control provided by dedicated units. The reaction temperature was monitored using a K-type thermocouple positioned at the center of the reactor. The temperature and pressure conditions in this work are 675–1,075 K and 1 atm, respectively. Hexanes (*n*-hexane, 3-methylpentane, 2,3-dimethylbutane, and 2-methylpentane) with a purity of 99% were purchased from Shanghai Titan Technology Co., Ltd (Shanghai, China), while argon (99.999% purity) was provided by Air Liquide (Shanghai) Co., Ltd (Shanghai, China). The total flow rate of all experiments was kept at 1,000 standard cubic centimeter per minute (SCCM) with the fuel and argon inlet mole fractions of 1% and 99% respectively. Pyrolysis products were analyzed using an online gas chromatograph (Agilent 7890B) fitted with two flame ionization detectors (FIDs). The FIDs, coupled with GS-Alumina capillary columns, were employed to quantify hydrocarbons, primarily C_1-C_4 species in this study. Following the methods in previous work[38,39], the mole fraction of pyrolysis products was determined using both the direct calibration method with standard gas mixtures and the indirect effective carbon number approach, based on the FID response. The uncertainties in mole fraction measurements are estimated to be ± 15% for direct calibration with standard gases, and ± 20% for the indirect calibration using the fuel[38,40,41], respectively.

Laminar burning velocity

The laminar flame propagation of hexane/air mixtures were investigated in a high-temperature, high-pressure combustion vessel. The related description of the experimental facility can be referred to in detail to our previous work[42]. In brief, the experimental facility mainly includes an injection system, a premixing vessel (an inner volume of 9.06 L), a cylindrical combustion vessel (an inner volume of 2.77 L), a spark ignition system, a temperature control system, a pressure control system, and a schlieren system. In the experiment, the synthetic air was provided by Air Liquide (Shanghai) Co., Ltd, while hexanes (*n*-hexane, 3-methylpentane, 2,3-dimethylbutane, and 2-methylpentane) with a purity of 99% were purchased from Shanghai Titan Technology Co., Ltd. The fuel vapor and synthetic air ($21\%O_2/79\%N_2$) were first mixed in the premixing vessel at a given equivalence ratio by using the partial pressure method. The definition of the stoichiometric reaction is $C_6H_{14} + 9.5(O_2 + 3.76N_2) = 6CO_2 + 7H_2O$. The prepared combustible mixtures were ignited by a spark generated at the center of the combustion vessel. The experiments of hexanes were performed at T_u = 373 K, P_u = 1–10 atm, and ϕ = 0.7–1.5. All the related systems were heated to 373 K to prevent fuel condensation. The propagation of spherical flames was recorded using a high-speed camera (Phantom V310), which was operated at 12,000 fps with a resolution of 480 × 480 pixels (corresponding to 75 × 75 mm^2 region). The flame radius range was chosen to be 10–23 mm to eliminate the impact of ignition and confinement[43–45] on flame propagation. The data processing and uncertainty evaluation methods are outlined in detail in our previous work[39,42]. Uncertainties from radiation, flame radius determination, repeatability, extrapolation/fitting, temperature, and pressure are considered. The uncertainty of the inlet temperature and inlet pressure are ± 1 K and ± 0.2 kPa, respectively.

Kinetic model

In this work, a comprehensive intermediate-to-high-temperature kinetic model of four hexane isomers containing 288 species and 2,179 reactions was proposed. The C_0-C_4 core mechanism was adopted from our propanol[7], propanal[35], and butane-2,3-dione[46] models. The C_5 sub-mechanism was derived from the model for pentane isomers[18]. The sub-mechanism of the four hexane isomers was mainly adopted from the work of Zhang et al.[12] with several important reactions updated based on the latest theoretical study, which is detailed in Supplementary Table S1. Thermodynamic data and transport data of C_0-C_4 species and C_5 species were obtained from our recent models of propanol[7], and the pentane isomers model[18], respectively. Thermodynamic data and transport data of species involved in the sub-mechanism of the four hexane isomers were adapted from Zhang et al.[12].

The present model incorporates H-atom abstraction reactions for n-hexane (NC_6H_{14}), 2-methylpentane (IC_6), 3-methylpentane (I_3C_6), and 2,3-dimethylbutane (XC_6), involving radicals such as H, CH_3, OH, HO_2, O, O_2, CH_3O, C_2H_3, and C_2H_5. The rate constants for H-atom abstraction reactions by H-atoms from n-hexane (R1–R3, see in

Supplementary Table S1), 2-methylpentane (R10–R14), 3-methylpentane (R25–R28), and 2,3-dimethylbutane (R37–R38) were derived from analogous reactions of n-butane (nC_4H_{10}), and i-butane (iC_4H_{10}), based on theoretical calculations and shock tube experiments conducted by Peukert et al.[47], while those by CH_3 for *n*-hexane (R4–R6), 2-methylpentane (R15–R19), 3-methylpentane (R29–R32), and 2,3-dimethylbutane (R39–R40) were adopted from the work of Orme et al.[48] and Goos et al.[49]. In addition, the rate constants for H-atom abstraction reactions by OH for *n*-hexane (R7–R9), 2-methylpentane (R20–R24) , 3-methylpentane (R33–R36), and 2,3-dimethylbutane (R41–R42) were adopted from the work of Badra et al.[50]. The consumption of hexyl radicals is governed by β-C scission reactions, i.e. β-C-C and β-C-H scission reactions, of which the rate constants were adopted from the work of Badra et al.[50].

Chemkin-PRO software[51] was adopted to perform all the simulations using the present model. Specifically, the simulation of adiabatic flame temperature (T_{ad}) was conducted using the Chemical and Phase Equilibrium module, the simulations of JSR was conducted using the Perfectly Stirred Reactor module, the simulation of IDTs was conducted using the Close Homogeneous Batch Reactor module, and the simulations of LBVs were conducted using the Premixed Laminar Flame Speed Calculation module with the consideration of the Soret effect. A refinement over a 10 cm domain (1,000 grid points, CURV 0.1, and GRAD 0.1) was applied to ensure proper convergence. The validation against experimental data of hexanes from previous literature[18,19,24,28,29,31] can be found in Supplementary Fig. S1–Fig. S5.

Results and discussion

Jet-stirred reactor pyrolysis

In the JSR pyrolysis experiments, a variety of pyrolysis products were identified, and their mole fractions were quantified as a function of temperature. Figures 2–5 show the comparison between the measured and simulated mole fraction distributions of fuels and detected products in the pyrolysis of *n*-hexane, 2,3-dimethylbutane, 3-methylpentane, and 2-methylpentane, respectively. The present model is shown to accurately predict fuel decomposition and the formation of the majority of pyrolysis products. The Zhang model[12] was also tested to simulate the JSR pyrolysis experiments. It is observed that the Zhang model[12] can generally capture the decomposition of n-hexane and the formation of most of its pyrolysis products, while under-predict the decomposition of the other three hexanes and the formation of most pyrolysis products.

To understand the pyrolysis chemistry of the hexane isomers, the ROP analysis was performed at about 85% fuel conversion, which corresponds to 1,025 K for *n*-hexane and 2-methylpentane and 1000 K for 3-methylpentane and 2,3-dimethylbutane. Under this fuel conversion, most of the pyrolysis products in *n*-hexane, 2,3-dimethylbutane, 3-methylpentane, and 2-methylpentane pyrolysis was abundantly produced. Figure 6 illustrates the primary reaction networks involved in the pyrolysis of the four hexane isomers at 1 atm, based on the rate of production (ROP) analysis.

Primary decomposition of hexane isomers

Figures 2a, 3a, 4a, & 5a show the fuel decomposition results in the pyrolysis of *n*-hexane, 2-methylpentane, 3-methylpentane, and 2,3-dimethylbutane. Slight differences in decomposition trends among the four fuels can be observed. The ROP analysis reveals that hexanes are primarily consumed through two reaction classes: bond dissociation and H-abstraction reactions. However, the relative contributions of these pathways differ depending on the fuel structure. Figure 7 compares the contributions of bond dissociation and H-abstraction reactions to the decomposition of the four hexane isomers. It is noticed that the contribution of bond dissociation reactions to fuel consumption decrease with the increase of branched structures in fuels. In *n*-hexane pyrolysis, a greater contribution of bond dissociation reactions is observed compared to the other three hexanes. Among bond dissociation reactions of *n*-hexane

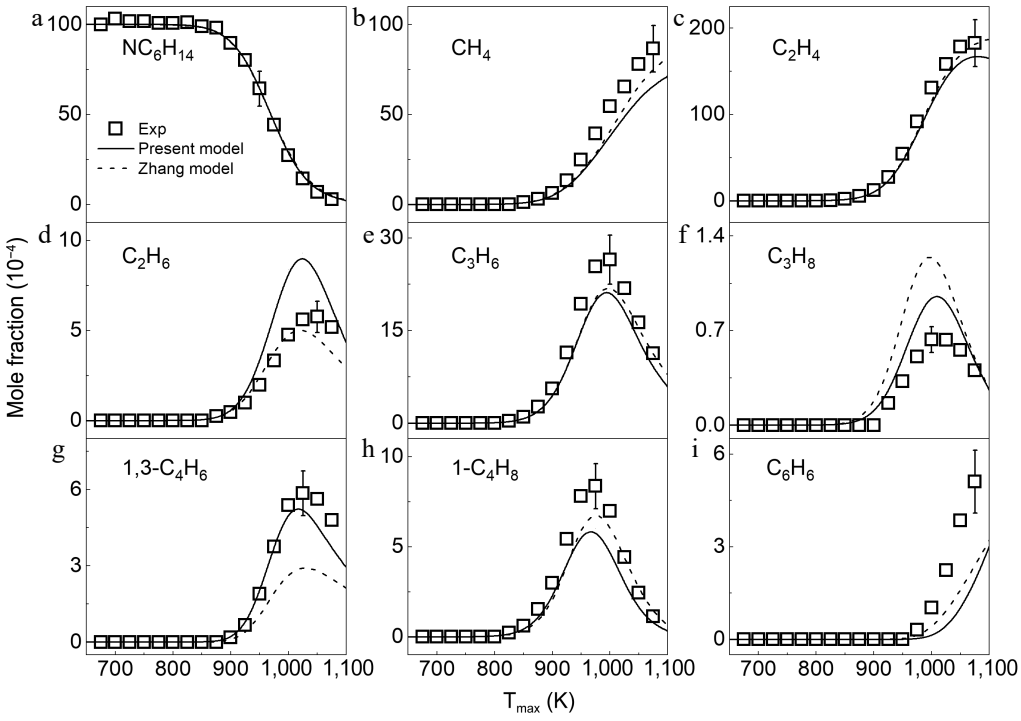

Fig. 2 Mole fraction distributions of *n*-hexane and products in *n*-hexane pyrolysis at 1 atm. Symbols and lines denote the measured and simulated results, respectively.

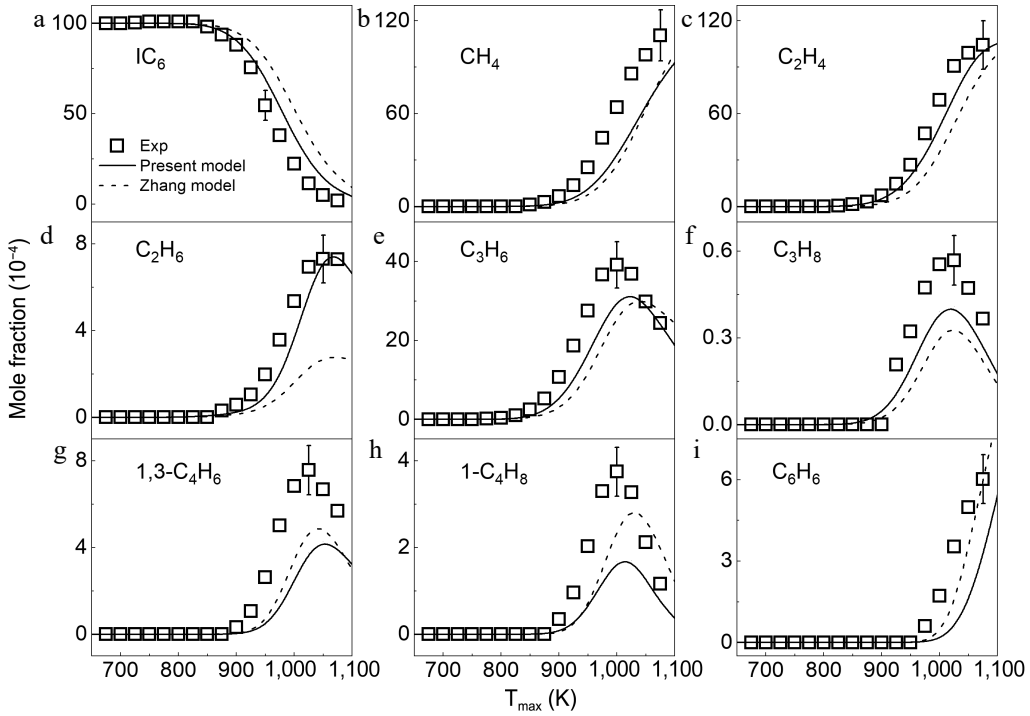

Fig. 3 Mole fraction distributions of 2-methylpentane and products in 2-methylpentane pyrolysis at 1 atm. Symbols and lines denote the measured and simulated results, respectively.

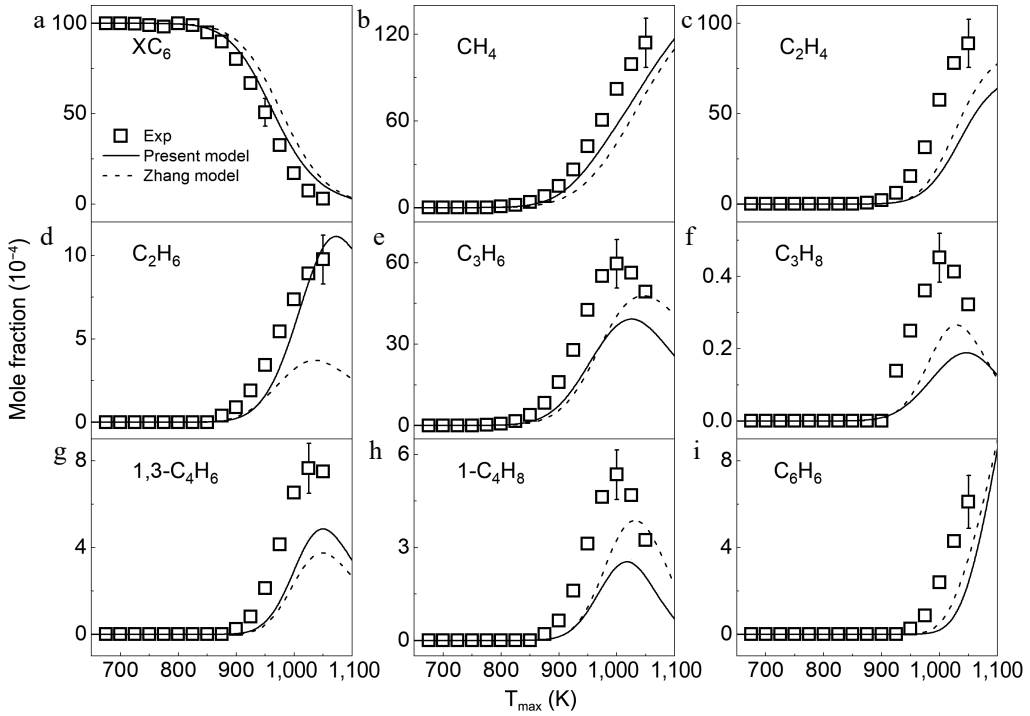

Fig. 4 Mole fraction distributions of 3-methylpentane and products in 3-methylpentane pyrolysis at 1 atm. Symbols and lines denote the measured and simulated results, respectively.

(R43–R45), two secondary-secondary C-C bond dissociation reactions (R43 and R44) producing two *n*-propyl (NC_3H_7), ethyl (C_2H_5), and 1-butyl (PC_4H_9) respectively contribute the most due to the lower BDEs. As for 2-methylpentane, the primary-tertiary C-C bond dissociation reaction (R46) contribute slightly more than the secondary-tertiary C-C bond dissociation reaction (R47) in 2-methylpentane pyrolysis. As for bond dissociation reactions of 3-methylpentane (R48–R50), the secondary-tertiary C-C bond dissociation reaction (R48) producing C_2H_5 and 2-butyl (SC_4H_9) contributes the most due to its lowest BDE. As for 2,3-dimethylbutane, the tertiary-tertiary C-C bond dissociation reaction (R51) producing two *i*-propyl (IC_3H_7) contribute far more than the primary-tertiary C-C dissociation reaction (R52) in 2,3-dimetylbutane pyrolysis because of its lower BDE.

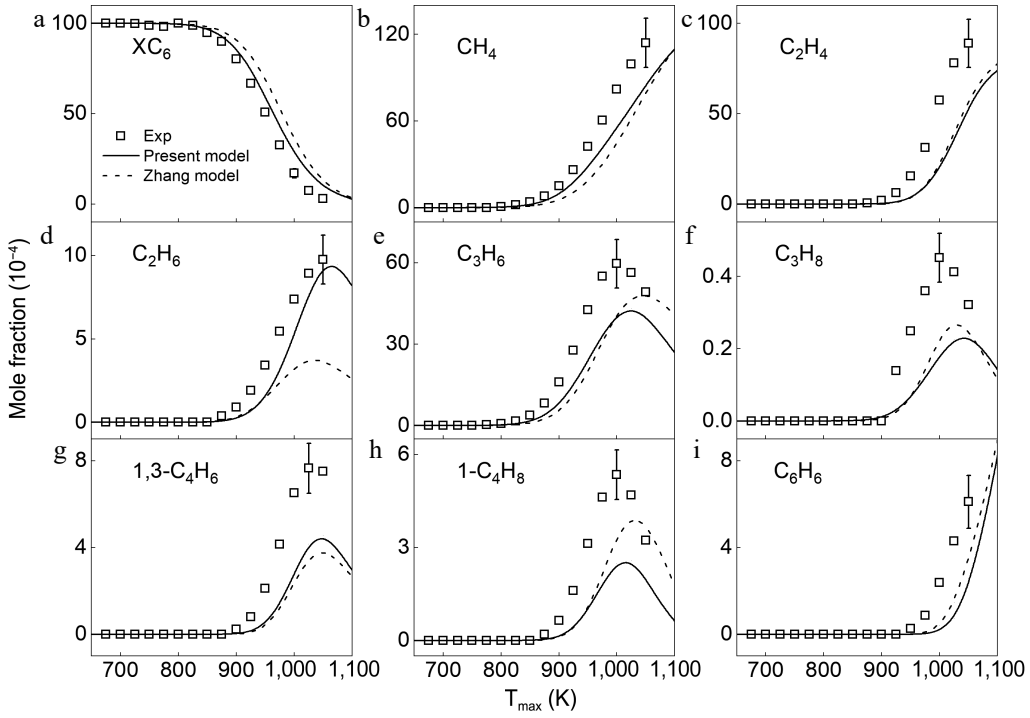

Fig. 5 Mole fraction distributions of 2,3-dimethylbutane and products in 2,3-dimethylbutane pyrolysis at 1 atm. Symbols and lines denote the measured and simulated results, respectively.

$$NC_6H_{14} = NC_3H_7 + NC_3H_7 \quad (R43)$$

$$NC_6H_{14} = C_2H_5 + PC_4H_9 \quad (R44)$$

$$NC_6H_{14} = CH_3 + C_5H_{11}\text{-}1 \quad (R45)$$

$$IC_6 = CH_3 + C_5H_{11}\text{-}2 \quad (R46)$$

$$IC_6 = NC_3H_7 + IC_3H_7 \quad (R47)$$

$$I3C_6 = SC_4H_9 + C_2H_5 \quad (R48)$$

$$I3C_6 = CH_3 + C_5H_{11}\text{-}3 \quad (R49)$$

$$I3C_6 = CH_3 + AC_5H_{11} \quad (R50)$$

$$XC_6 = IC_3H_7 + IC_3H_7 \quad (R51)$$

$$XC_6 = CH_3 + CC_5H_{11} \quad (R52)$$

It is also known that H-abstraction reactions play a more crucial role in fuel consumption than bond dissociation reactions due to more radicals produced at higher temperatures. H and CH_3 are two major radials participating in H-abstraction reactions with four hexane isomers. It is well-established that the dissociation energies of C-H bonds reduce in the order of primary, secondary, and tertiary carbon sites. As a result, the H atom on a secondary carbon site is more readily abstracted than that on a primary carbon site. Consequently, H-abstraction reactions on the secondary carbon site (R2–R3 and R5–R6) contribute more to the consumption of n-hexane than those on the primary carbon site (R1 and R4). For 2-methylpentane, the H-abstraction reactions on the tertiary carbon site (R11 and R16) have the greatest contribution, due to the lower bond dissociation energies (BDEs) at these sites. In the case of 3-methylpentane, H-abstraction reactions on the secondary carbon site (R26 and R30) play a more significant role in the consumption of 3-methylpentane compared to those on the primary carbon site (R25, R28–R29, and R32) and tertiary carbon site (R27 and R31). For 2,3-dimethylbutane, the higher number of H-atoms on the primary carbon site, six times greater than those on the tertiary carbon site-leads to a greater contribution from H-abstraction reactions on the primary carbon site (R37 and R39) compared to the tertiary site (R38 and R40). Additionally, ROP analysis reveals that H-abstraction reactions by CH_3 radicals (R39 and R40) make a significantly larger contribution to the consumption of 2,3-dimethylbutane than those by H-atoms (R37 and R38). In contrast, for the other three hexane isomers, H-abstraction reactions by H-atoms contribute more than those involving CH_3 radicals. This discrepancy can be attributed to the highly branched structure of 2,3-dimethylbutane, which favors the production of CH_3 radicals during pyrolysis.

Fuel isomeric effects on pyrolysis products in hexane isomers

Alkanes and benzene

C_1-C_3 alkanes and benzene were measured in the pyrolysis of the four hexane isomers, as shown in Figs 2–5. The measured peak mole fractions of CH_4, C_2H_6 and benzene (C_6H_6) are compared in Fig. 8, which indicates a pronounced fuel isomeric effect on concentrations of pyrolysis products. CH_4 and C_2H_6 are two major alkane products in the pyrolysis of the four hexane isomers, which are strongly related to CH_3 radical. Based on ROP analysis, H-abstraction reactions of CH_3 through fuels or $CH_3 + H = CH_4$ together contribute to CH_4 production, and the production of C_2H_6 in four hexane isomers pyrolysis are mainly contributed by the self-recombination reaction of CH_3 (R52). Among the pyrolysis of four hexane isomers, it is observed that 2,3-dimethylbutane yields the highest CH_4 and C_2H_6 concentration, while *n*-hexane pyrolysis produces the lowest CH_4 and C_2H_6. It can be explained by the molecular structure of 2,3-dimethylbutane, which has four CH_3 groups. It is seen that the C_6H_6 concentration is highest in pyrolysis of 2,3-dimethylbutane and lowest in pyrolysis of *n*-hexane among the four hexane isomers pyrolysis. The propargyl radical is known as an important precursor of benzene[52] and its most abundant formation in 2,3-dimethylbutane pyrolysis explains the highest concentration levels of benzene.

$$2CH_3(+M) = C_2H_6(+M) \quad (R52)$$

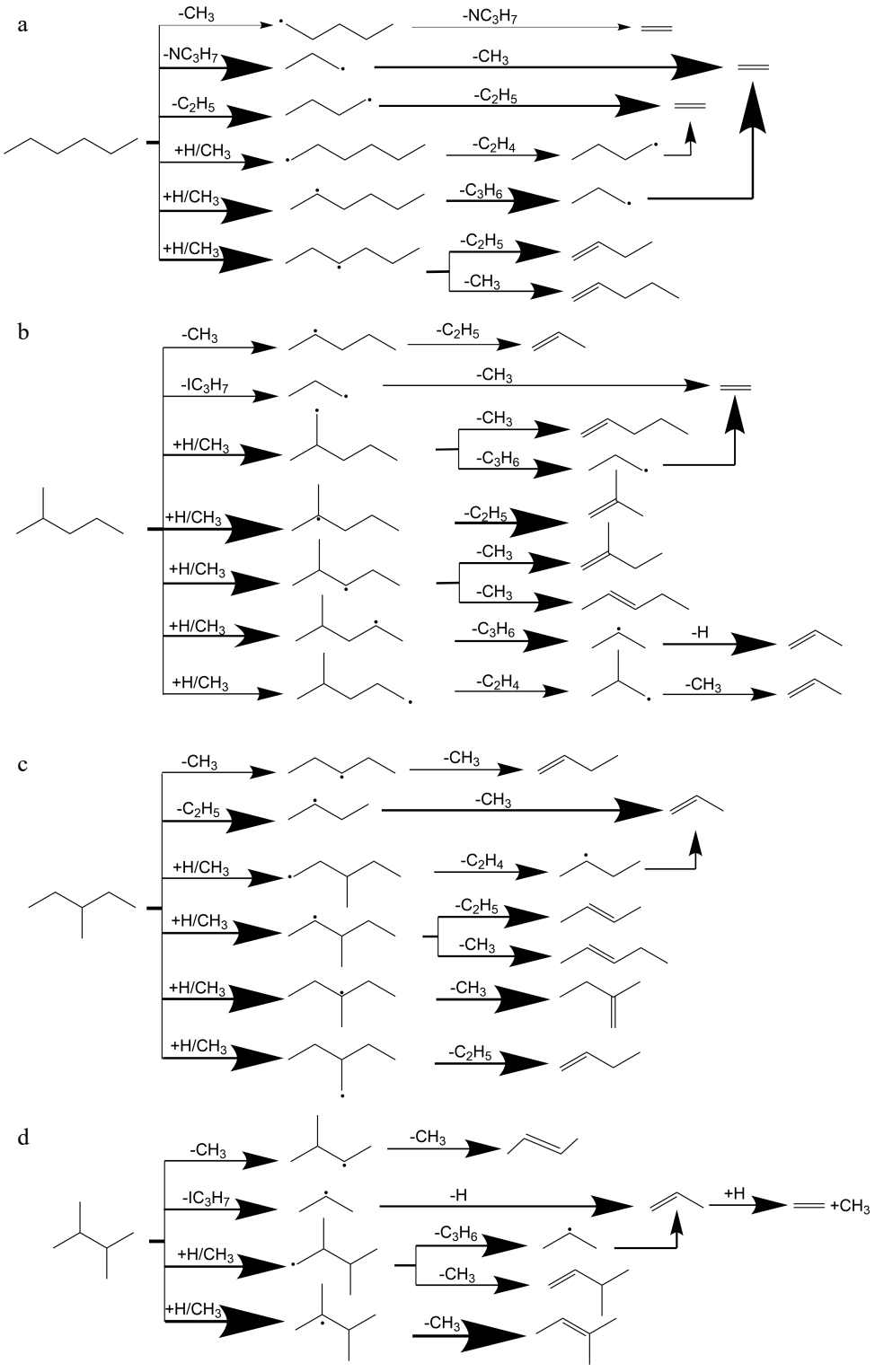

Fig. 6 The primary reaction networks of (a) *n*-hexane at 1,025 K, (b) 2-methylpentane at 1,025 K, (c) 3-methylpentane at 1,000 K, and (d) 2,3-dimethylbutane at 1,000 K. The numbers represent the percentages of carbon fluxes for the corresponding reactions.

Alkenes

C_2-C_4 alkenes were measured in the pyrolysis of the four hexane isomers, as shown in Figures 2–5. Figure 9 compares the experimental peak mole fractions of C_2H_4, C_3H_6, and 1-butene (1-C_4H_8). It can be observed that alkenes, especially the concentration of C_2H_4 and C_3H_6 have significant differences in the four hexane isomer pyrolysis. *n*-Hexane pyrolysis produces the largest C_2H_4 concentration and the smallest C_3H_6 concentration among the four hexane isomers pyrolysis, while 2,3-dimethylbutane pyrolysis yields the largest C_3H_6 concentration and the lowest C_2H_4 concentration. ROP analysis indicates that the β-C-C or β-C-H scission reactions of C_2-C_4 n-alkyl radicals (R53-R55), generated from fuel decomposition, account for nearly 85% of the C_2H_4 production in n-hexane pyrolysis. Among the three *n*-alkyl radicals, NC_3H_7 is mainly formed from R43 and the β-C-C scission reaction of 2-hexyl (C_6H_{13}-2) radical (R56), while C_2H_5 can be formed from R44, R55 and the β-C-C scission reaction of

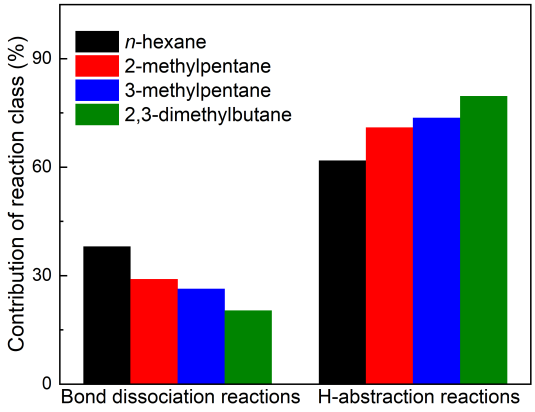

Fig. 7 Contributions of bond dissociation reactions and H-abstraction reactions to fuel consumption in hexanes pyrolysis at 1 atm, 1,075 K (for *n*-hexane and 2-methylpentane) and 1,050 K (for 3-methylpentane and 2,3-dimethylbutane).

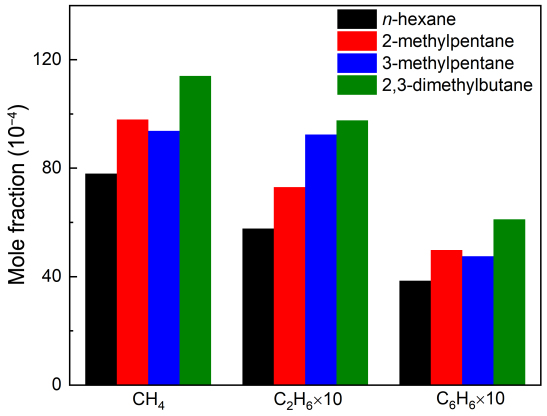

Fig. 8 Comparisons of experimental maximum mole fractions of methane, ethane, and benzene in *n*-hexane, 2-methylpentane, 3-methylpentane, and 2,3-dimethylbutane pyrolysis at 1 atm. For methane and benzene, the temperature is 1,075 K for *n*-hexane and 2-methylpentane, and 1,050 K for 3-methylpentane and 2,3-dimethylbutane. For ethane, the temperature is 1,050 K for four hexanes.

3-hexyl (C_6H_{13}-3) radical (R57). As a result, C_2H_4 attracts the majority of the carbon flux from n-hexane, which explains the highest concentration of C_2H_4 among the four hexane isomers. The concentration of C_3H_6 is lowest in *n*-hexane pyrolysis among the four hexane isomers, because its main production pathway is only R56, which has the lowest carbon flux from *n*-hexane. In contrast, C_3H_6 is the dominant alkene product in 2,3-dimethylbutane pyrolysis. According to ROP analysis, the β-C-H scission reaction of IC_3H_7 (R58) and the β-C-C scission reaction of 2,3-dimethyl-1-butyl (XC_6-1) radical (R59) contribute nearly 95% together to the production of C_3H_6 in the pyrolysis of 2,3-dimethylbutane, which has the greatest carbon flux from 2,3-dimethylbutane. Therefore, the concentration of C_3H_6 is highest in 2,3-dimethylbutane pyrolysis. However, the formation of C_2H_4 is mainly through the decomposition of C_3H_6 (R60), which can explain the lowest C_2H_4 concentration in 2,3-dimethylbutane among the four hexane isomers pyrolysis.

$$NC_3H_7 = C_2H_4 + CH_3 \quad (R53)$$

$$C_2H_5(+M) = C_2H_4 + H(+M) \quad (R54)$$

$$PC_4H_9 = C_2H_4 + C_2H_5 \quad (R55)$$

$$C_6H_{13}-2 = C_3H_6 + NC_3H_7 \quad (R56)$$

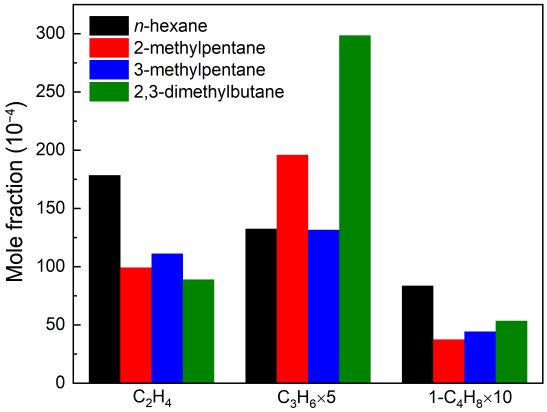

Fig. 9 Comparisons of experimental maximum mole fractions of ethylene, propene, and 1-butene in *n*-hexane, 2-methylpentane, 3-methylpentane, and 2,3-dimethylbutane pyrolysis at 1 atm. For ethylene, the temperature is 1075 K for *n*-hexane and 2-methylpentane, and 1050 K for 3-methylpentane and 2,3-dimethylbutane. For propene and 1-butene, the temperature is 1000 K for four hexanes.

$$C_6H_{13}-3 = C_2H_5 + 1-C_4H_8 \quad (R57)$$

$$IC_3H_7 = C_3H_6 + H \quad (R58)$$

$$XC_6-1 = C_3H_6 + IC_3H_7 \quad (R59)$$

$$C_3H_6 + H = C_2H_4 + CH_3 \quad (R60)$$

The concentrations of C_2H_4 in 2-methylpentane and 3-methylpentane pyrolysis are close, which are located in the middle among the four hexanes pyrolysis. A slightly higher concentration of C_3H_6 in 2-methylpentane pyrolysis is observed than that in 3-methylpentane pyrolysis. Based on ROP analysis, the β-C-C scission reaction of 2-methyl-4-pentyl (IC_6-4) radical (R61), 2-methyl-1-pentyl (IC_6-1) radical (R62), 2-pentyl (C_5H_{11}-2) radical (R63), and *i*-butyl (IC_4H9) radical (R64) and R58 together contribute around 90% to the production of C_3H_6 in the pyrolysis of 2-methylpentane, while the β-C-C scission reaction of SC_4H_9 (R65) and the addition-elimination reactions of 2-butene (2-C_4H_8) (R66) and 1-C_4H_8 (R67) contribute around 90% together to the formation of C_3H_6 in 3-methylpentane pyrolysis. The carbon flux from 2-methylpentane to C_3H_6 is higher than the carbon flux from 3-methylpentane to C_3H_6, which explains the concentration of C_3H_6 in 2-methylpentane pyrolysis is larger than that in 3-methylpentane pyrolysis.

$$IC_6-4 = C_3H_6 + IC_3H_7 \quad (R61)$$

$$IC_6-1 = C_3H_6 + NC_3H_7 \quad (R62)$$

$$C_5H_{11}-2 = C_3H_6 + C_2H_5 \quad (R63)$$

$$IC_4H_9 = C_3H_6 + CH_3 \quad (R64)$$

$$SC_4H_9 = C_3H_6 + CH_3 \quad (R65)$$

$$2-C_4H_8 + H = C_3H_6 + CH_3 \quad (R66)$$

$$1-C_4H_8 + H = C_3H_6 + CH_3 \quad (R67)$$

Figure 9 also shows the mole fractions of 1-C_4H_8 in *n*-hexane pyrolysis is the highest among the four hexane isomers pyrolysis. Based on ROP analysis, R57 and the combination of allyl (C_3H_5-A) and CH_3 (R68) are the major production pathway of 1-C_4H_8 in *n*-hexane pyrolysis, while R68 is the major formation pathway of 1-C_4H_8 in other three hexanes. The ability to produce allyl and CH_3 radicals of 2,3-dimethylbutane explains the slightly higher concen-

tration of 1-C_4H_8 among the three branched hexane isomers.

$$C_3H_5\text{-A} + CH_3(+M) = 1\text{-}C_4H_8(+M) \quad \text{(R68)}$$

Laminar burning velocity

Experimental and simulated results

In this work, LBVs of *n*-hexane/air, 2-methylpentane/air, 3-methylpentane/air, and 2,3-dimethylbutane/air mixtures at T_u = 373 K and P_u = 1, 2, 5, and 10 atm were measured, which is shown in Fig. 10. A decreasing trend of LBVs of the four hexane isomers can be observed as initial pressures increase. The maximum LBV values of the four hexane isomers exist at around ϕ = 1.1 at 1 and 2 atm, while the effective LBV values can only be obtained at ϕ = 0.7–1.1, and ϕ = 0.7–1.0 under 5 and 10 atm respectively due to the strong effect of cellular instability. The present model can capture the measured LBVs of the four hexane isomers well under all investigated conditions.

Figure 11 presents the measured Markstein lengths of *n*-hexane/air, 2-methylpentane/air, 3-methylpentane/air, and 2,3-dimethylbutane/air mixtures at T_u = 373 K and P_u = 1, 2, 5 and 10 atm. As the equivalence ratio increases, the Markstein lengths for the four hexane isomers decrease across all investigated conditions, with a transition from positive to negative values occurring at ϕ = 1.3 for both 1 and 2 atm. At a given equivalence ratio, it is observed that the Markstein length decreases with increasing pressure when ϕ < 1.4, whereas the opposite trend is observed at ϕ = 1.5 and pressures of 1 and 2 atm. Overall, the similar trends in Markstein length suggest comparable flame instability characteristics among the four hexane isomers.

The comparisons between the measured and simulated results of the four hexane isomers at 373 K and 1 atm by the present model and the previous model proposed by Zhang et al.[12] (named as the Zhang model) were also performed, as shown in Fig. 12. The Zhang model[12] can well predict the measured LBVs of *n*-hexane and 3-methylpentane under lean and stoichiometric conditions, but it under-predicts the measured LBVs under rich conditions with the largest difference up to 5 cm/s. As seen from Fig. 12a & d, the Zhang model[12] under-predicts the measured LBVs of 2-methylpentane and 2,3-dimethylbutane under lean, stoichiometric, and rich conditions. Compared with the Zhang model[12], the present model is generally good under all the investigated equivalence ratios, especially under rich conditions.

Fuel-specific combustion chemistry of hexane flames

Figure 13 shows reaction schemes of primary decomposition pathways of the four hexane isomers in the lean and rich flame at 1 atm based on the rate of production (ROP) analysis. It can be seen that the H-abstraction reactions govern the consumption of the four fuels and further decomposition of the produced fuel radicals mainly continues *via* β-C-C scission reactions. *n*-hexane mainly produces 1-hexyl (C_6H_{13}-1), 2-hexyl (C_6H_{13}-2) and 3-hexyl (C_6H_{13}-3) through H-abstraction reactions under all equivalence ratios, while the C-C bond dissociation reaction forming NC_3H_7 and *n*-butyl (NC_4H_9) becomes more important under rich conditions. Subsequent decomposition of these intermediates tends to produce a significant amount of C_2H_4 and C_2H_5, along with smaller quantities of C_3H_6 and CH_3. NC_3H_7, formed through C-C bond dissociation of 2-methylpentane, along with the five fuel radicals produced from H-abstraction reactions, primarily generates large amounts of C_3H_6 and CH_3, with limited production of C_2H_4 and C_2H_5. In contrast, SC_4H_9, arising from the C-C bond dissociation of 3-methylpentane, along with the four fuel radicals from H-abstraction reactions, leads to the abundant formation of C_2H_4 and C_2H_5, while substantial quantities of C_3H_6 and CH_3 are also produced in the 3-methylpentane flame. For 2,3-dimethylbutane, H-abstraction reactions at both the primary and tertiary carbon sites dominate fuel consumption, with the remaining fuel consumed by the C-C bond dissociation reaction forming IC_3H_7. Further decomposition of these intermediates results in the production of significant amounts of C_3H_6 and CH_3.

The sensitivity analysis results in Figs 14 & 15 reveal that most of the highly sensitive reactions are similar across the flames of the four fuels with C_0-C_2 reactions consistently dominating. Among them, the chain branching reaction between H and O_2 (H + O_2 = O + OH) exhibits the highest positive sensitivity coefficients. The chain propagation reaction CO + OH = CO_2 + H is of secondary importance under lean conditions but becomes less significant under rich conditions because of the reduced availability of OH[6]. Two pressure-dependent reactions play crucial roles under different

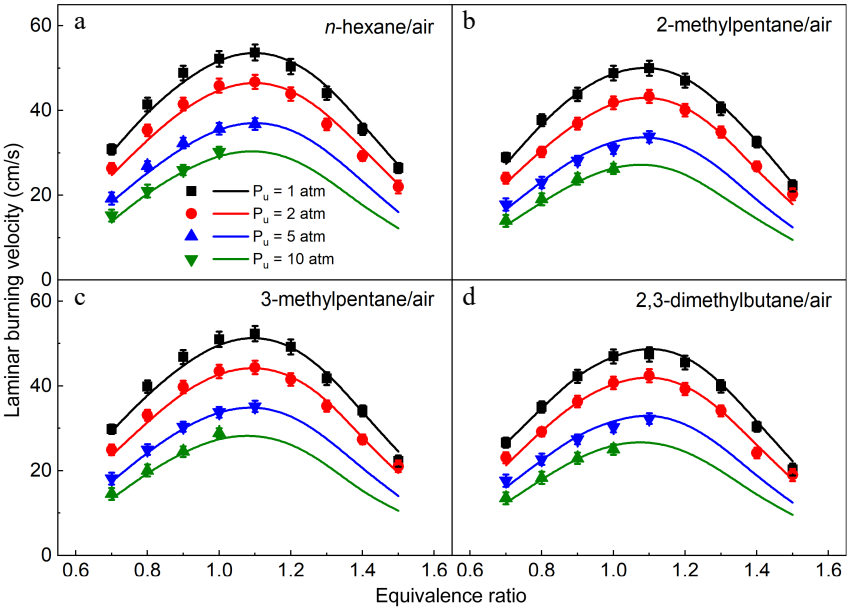

Fig. 10 Laminar burning velocities of (a) *n*-hexane/air, (b) 2-methylpentane/air, (c) 3-methylpentane/air, and (d) 2,3-dimethylbutane/air mixtures at 1-10 atm and 373 K. Symbols and lines denote the measured and simulated results, respectively.

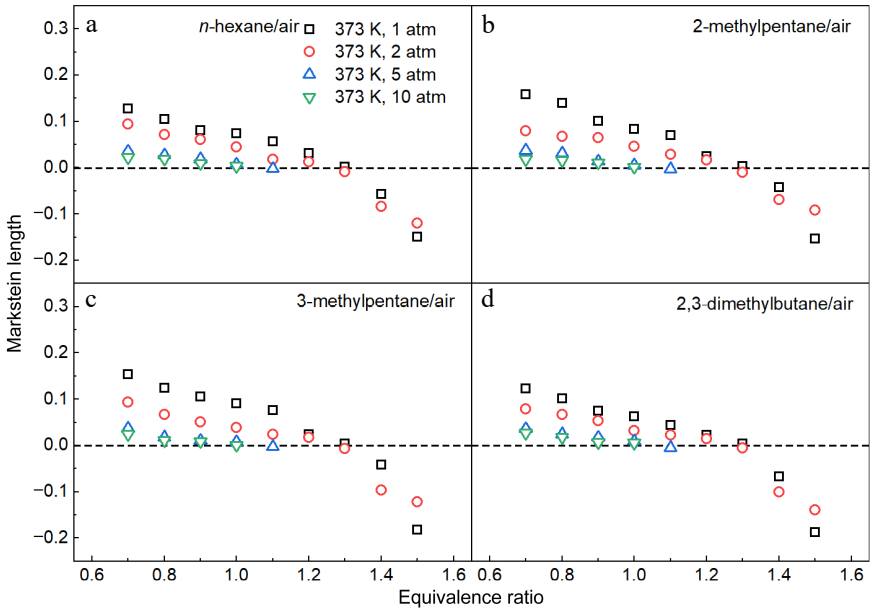

Fig. 11 Measured Markstein lengths of (a) *n*-hexane/air, (b) 2-methylpentane/air, (c) 3-methylpentane/air, and (d) 2,3-dimethylbutane/air mixtures at 1-10 atm and 373 K.

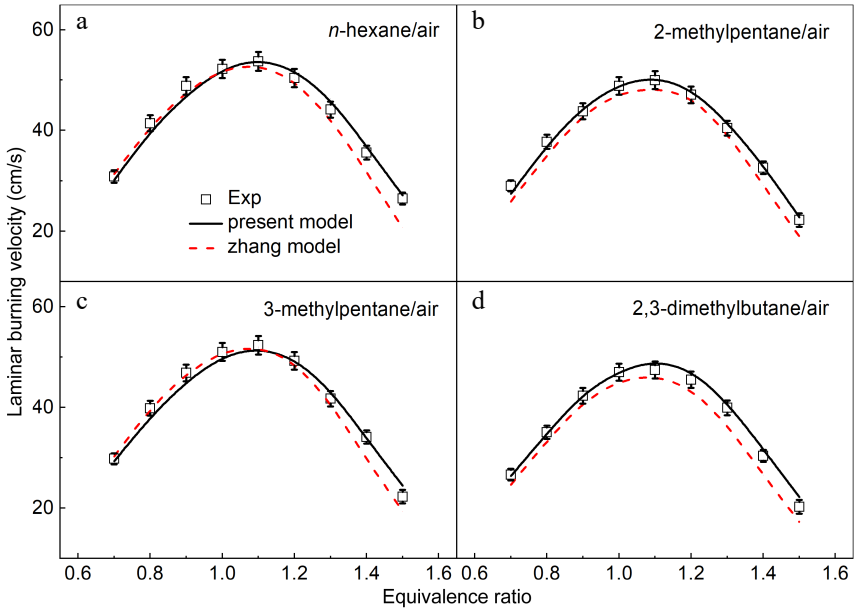

Fig. 12 Laminar burning velocities of (a) *n*-hexane/air, (b) 2-methylpentane/air, (c) 3-methylpentane/air, and (d) 2,3-dimethylbutane/air mixtures at 1 atm and 373 K. Symbols denote the measured results. Solid lines and dotted lines denote the simulated results by the present model and the Zhang model[12].

conditions: the chain inhibition reaction H + O_2 (+M) = HO_2 (+M) is significant under lean conditions, while the chain termination reaction CH_3 + H (+M) = CH_4 (+M) is critical under rich conditions. Additionally, key radicals associated with fuel decomposition pathways, particularly C_2H_5 and CH_3, are also evident in the most sensitive reactions.

Fuel isomeric effects on hexane flame propagations

Aiming to investigate the fuel isomeric effects on laminar flame propagation of the four hexane isomers, the measured LBVs of the four hexane isomers at P_u = 1–10 atm are compared in Fig. 16. Pronounced fuel isomeric effects can be observed in the LBVs of hexane isomers, following the order: *n*-hexane > 3-methylpentane > 2-methylpentane > 2,3-dimethylbutane. The reactivity of four hexane isomers found in LBV results is similar to the previous findings in IDTs[12]. In general, LBVs of the four hexane isomers decrease with the increase of the number of branched chains in the fuel molecule, which is comparable with previous observations for other alkanes[6,53].

Laminar flame propagation is well known to be influenced by thermal, transport, and kinetic effects[27]. Isomeric fuels with the same functional group provide an ideal framework for decoupling of these three effects. The transport effects can be negligible due to the similar molecular weight and similar Markstein lengths of the isomers. Furthermore, as shown in Fig. 17, the adiabatic flame temperatures of the four hexane isomers differ by less than 5 K. Consequently, the thermal effect is unlikely to explain the variations in LBV values among these isomers.

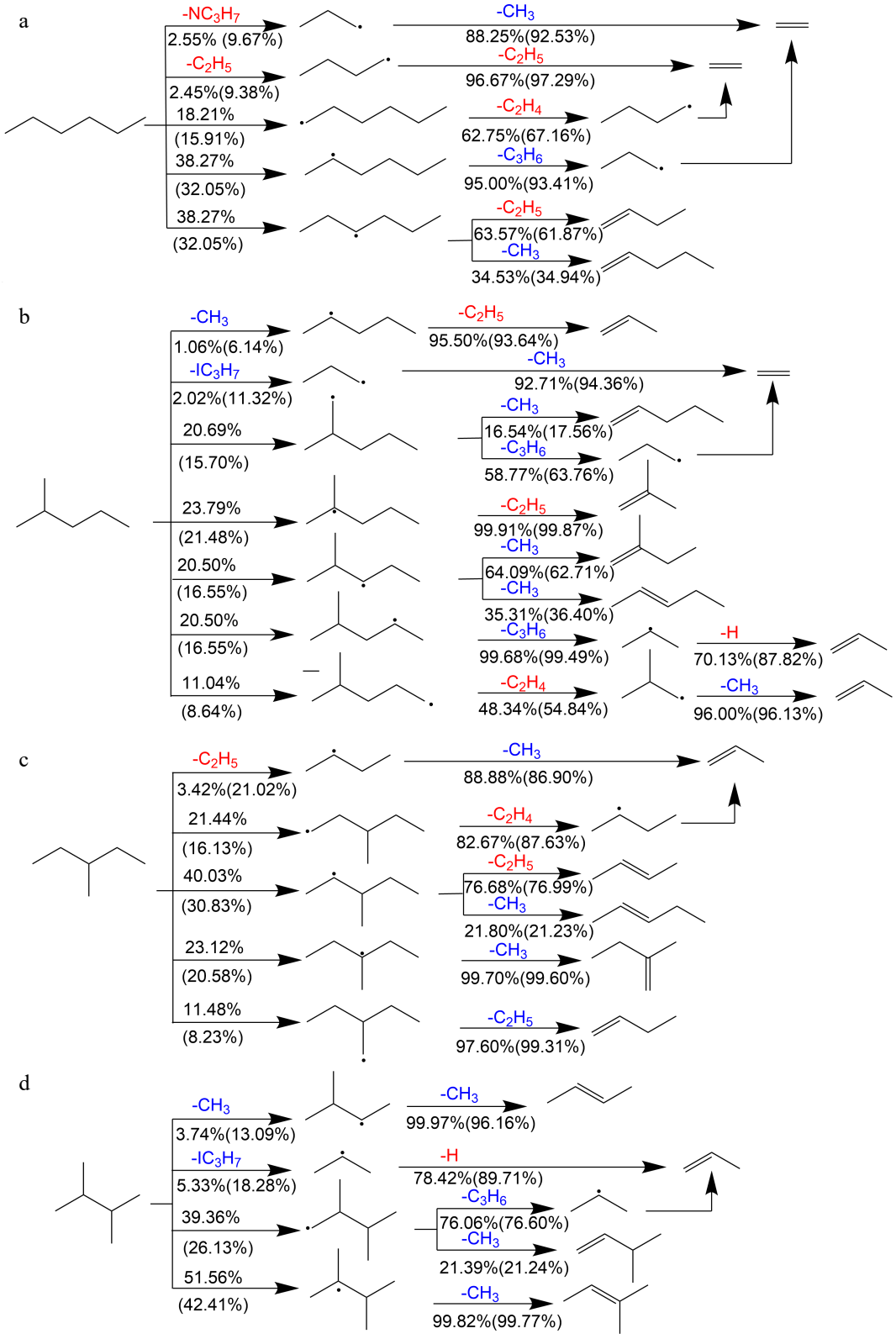

Fig. 13 Reaction schemes of primary decomposition pathways of (a) *n*-hexane, (b) 2-methylpentane, (c) 3-methylpentane, and (d) 2,3-dimethylbutane at 373 K, 1 atm, ϕ = 0.7 and 1.5. Red and blue highlight the intermediates which generally promotes and inhibits the flame propagation respectively. Numbers represent the percentages of corresponding pathways in total reaction flux (outside the brackets: ϕ = 0.7; in brackets: ϕ = 1.5).

It is well established that a fuel's reactivity is heavily influenced by its radical pool during combustion[8,9]. Figure 18 compares the simulated maximum mole fractions of CH_3, C_2H_5, C_2H_4, and C_3H_6 in rich (ϕ = 1.5) flames of the four hexane isomers at 373 K and 1 atm. Among the four isomers, the *n*-hexane flame has the lowest CH_3 concentration and the highest C_2H_5 concentration. However, the 2,3-dimethylbutane flame has the largest CH_3 concentration and the smallest C_2H_5 concentration among the four hexane isomers. According to the sensitivity analysis, CH_3 readily consume H through chain termination reaction producing methane, that is CH_3 + H (+M)

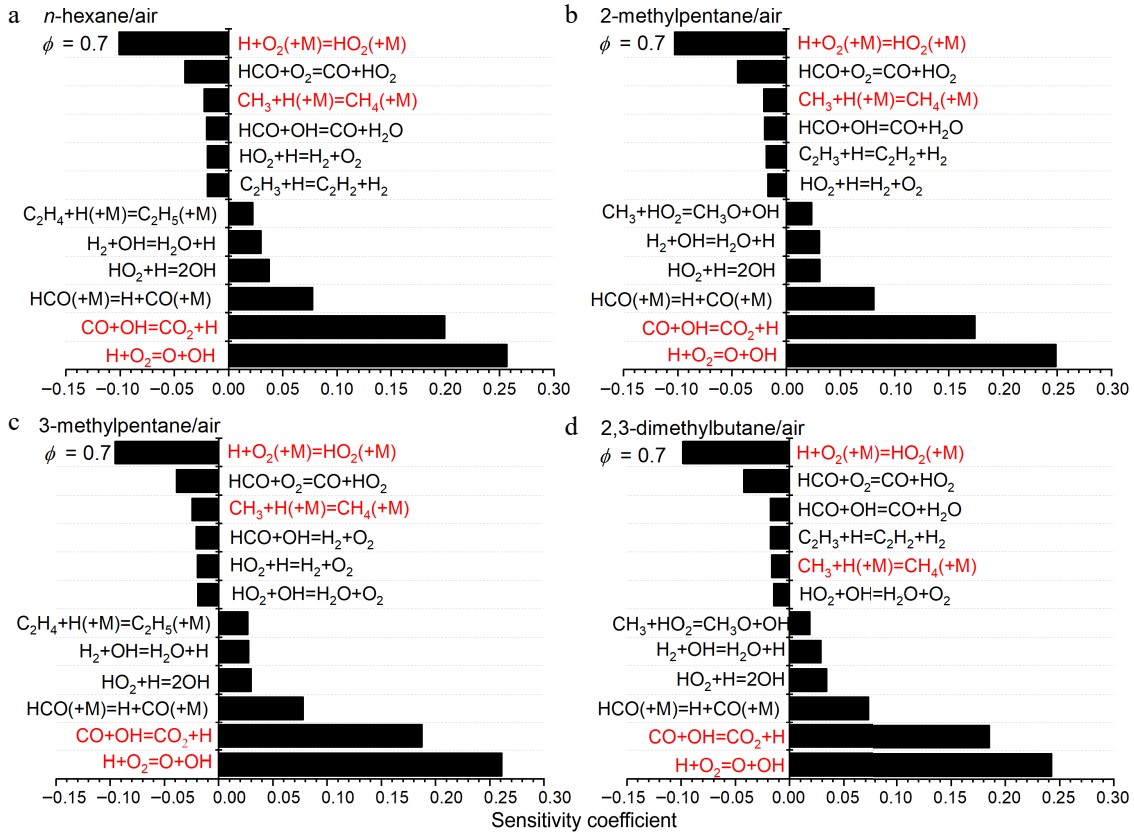

Fig. 14 Sensitivity analysis of LBVs for (a) *n*-hexane/air, (b) 2-methylpentane/air, (c) 3-methylpentane/air, and (d) 2,3-dimethylbutane/air at 373 K, 1 atm and $\phi = 0.7$. Some important reactions are highlighted in red.

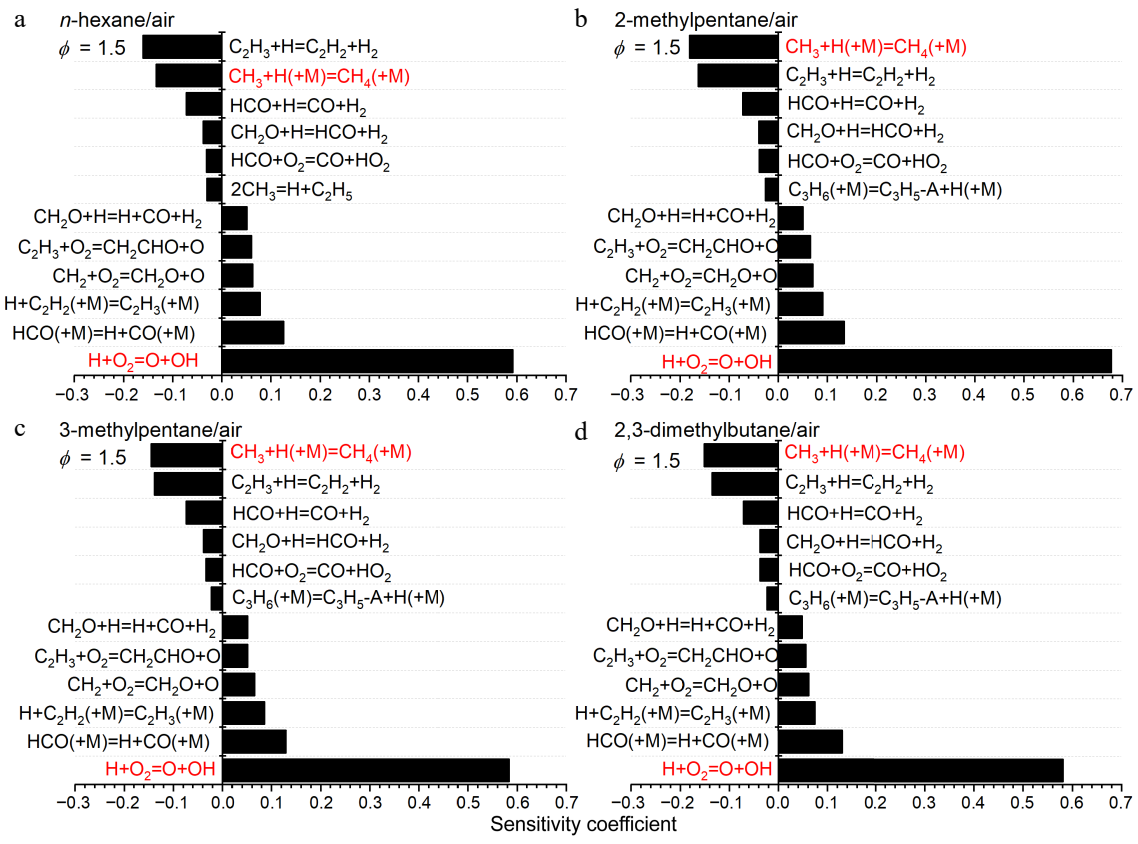

Fig. 15 Sensitivity analysis of LBVs for (a) *n*-hexane/air, (b) 2-methylpentane/air, (c) 3-methylpentane/air, and (d) 2,3-dimethylbutane/air at 373 K, 1 atm and $\phi = 1.5$. Some important reactions are highlighted in red.

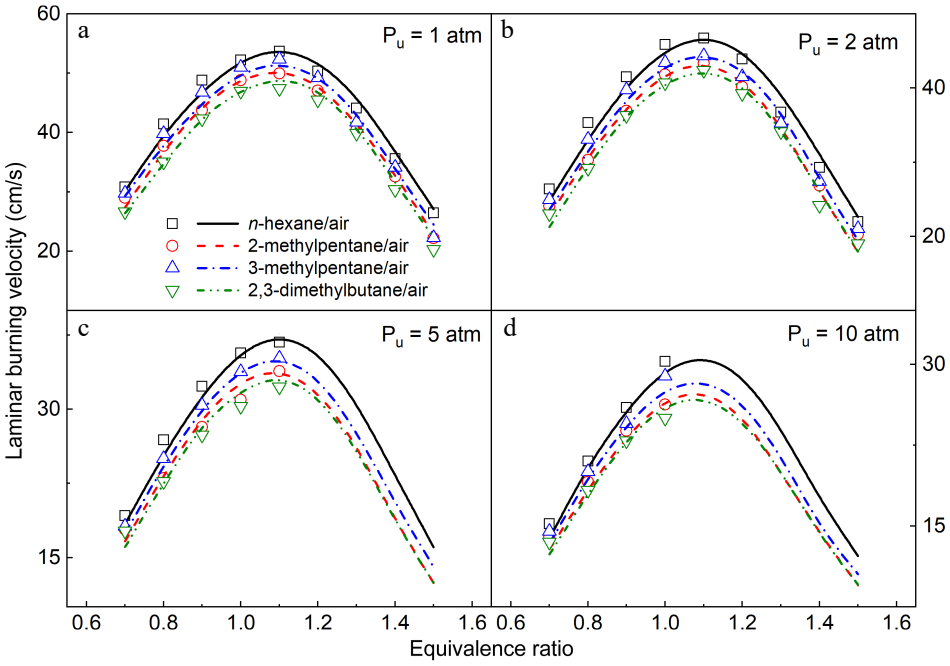

Fig. 16 Comparison of measured (symbols) and simulated (lines) LBVs of the four hexane isomers at 1–10 atm and 373 K.

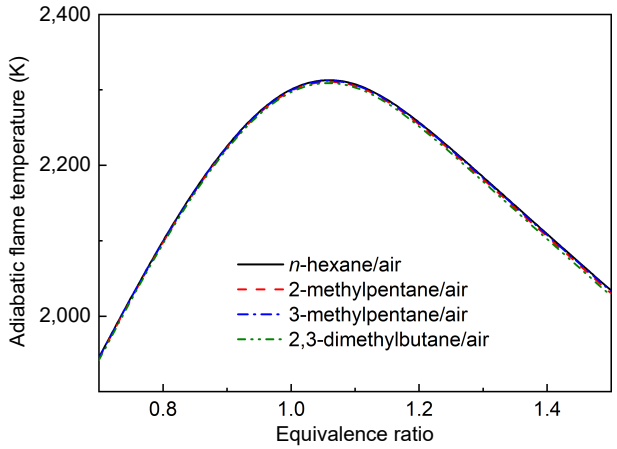

Fig. 17 Comparisons of calculated adiabatic flame temperatures of four hexanes flames at P_u = 1 atm.

= CH_4 (+M), which plays a key role in inhibiting laminar flame propagation. In contrast, C_2H_5 is prone to release H by β-C-H scission reaction, that is $C_2H_5 = C_2H_4 + H$, thereby promoting the laminar flame propagation. On the other hand, further decomposition reactions of the dominant products also have remarkable effects on the LBVs. Furthermore, the *n*-hexane flame has the largest C_2H_4 concentration and the smallest C_3H_6 concentration among the four hexane isomers. However, the 2,3-dimethylbutane flame has the largest C_3H_6 concentration and the smallest C_2H_4 concentration among the four hexane isomers. This is primarily due to the structural characteristic of 2,3-dimethylbutane that has only primary carbon and tertiary carbon atoms, thus it can easily form propene and methyl but hardly produces ethyl and ethylene, as shown in Fig. 13d. The fate of C_2H_4 is to produce relatively active vinyl (C_2H_3), while C_3H_6 can readily convert to stable C_3H_5-A. C_2H_3 and C_3H_5-A play crucial roles as H-producing and H-consuming agents forming acetylene (C_2H_2) and C_3H_6, promoting and inhibiting the laminar flame propagation respectively. As a result, *n*-hexane exhibits the strongest reactivity

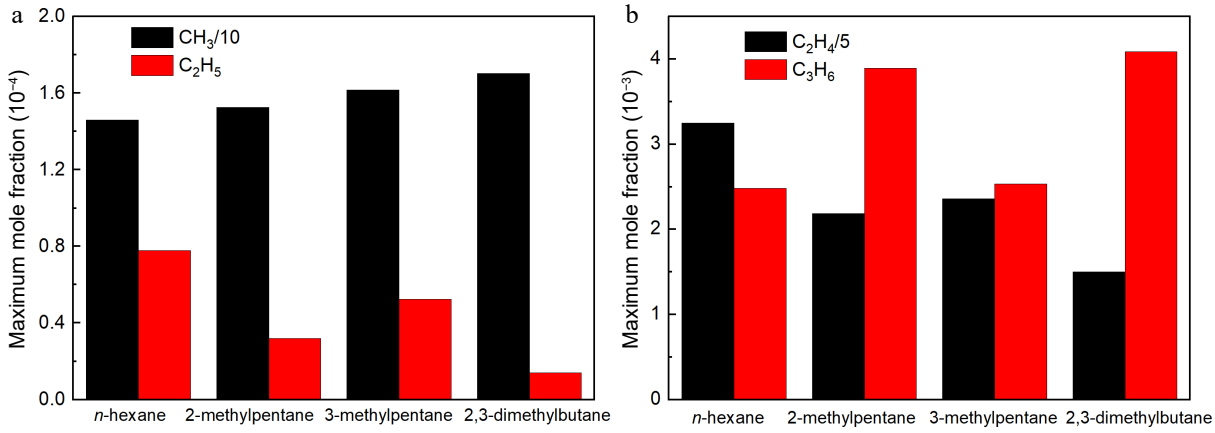

Fig. 18 Comparisons of simulated maximum mole fraction of critical radicals by the present model in *n*-hexane, 2-methylpentane, 3-methylpentane, and 2,3-dimethylbutane flames at 373 K, 1 atm and ϕ = 1.5: (a) methyl and ethyl, (b) ethylene and propene.

and the quickest flame propagation, whereas 2,3-dimethylbutane shows the weakest reactivity and the slowest flame propagation.

For 2-methylpentane and 3-methylpentane, it is observed that the location of branched methyl moiety in two fuels can also lead to differences in flame propagation. 3-methylpentane propagates slightly faster than 2-methylpentane under all investigated conditions. In 3-methylpentane flame, the C_2H_5 concentration is 64% higher than that of 2-methylpentane, while the CH_3 concentration is only 5% higher than that of 2-methylpentane. Therefore, the promotion effect of C_2H_5 to its flame propagation is more substantial than the inhibition effect of CH_3 to its flame propagation. Furthermore, the C_3H_6 concentration is much lower than that in 2-methylpentane flame, which can also inhibit laminar flame propagation. These can provide a certain explanation for the experimental phenomenon that the laminar flame propagation of 3-ethylpentane is quicker than that of 2-methylpentane.

Conclusions

This study investigated the pyrolysis and laminar burning velocities of four hexane isomers, that is *n*-hexane, 3-methylpentane, 2,3-dimethylbutane, and 2-methylpentane. The pyrolysis of the four hexane isomers was conducted using an atmospheric jet-stirred reactor with analysis performed using GC. Laminar burning velocities of four hexane/air mixtures were investigated at 373 K and 1, 2, 5, and 10 atm using the spherical flame propagation method. Distinct behaviors of the four hexane isomers were observed in both pyrolysis reactivity, product distributions, and laminar flame propagation. A comprehensive kinetic model for the four hexane isomers was proposed and subsequently validated through comparison with newly obtained experimental data.

Modeling analyses were conducted to understand the effects of fuel structure on the combustion behaviors among the four hexane isomers. Under pyrolysis conditions, unimolecular decomposition and H-abstraction reactions account for the majority of the fuel consumption. The highly branched structure of 2,3-dimethylbutane directs most of the carbon flux towards propene, whereas *n*-hexane prefers the formation of ethylene. This explains the highest concentrations of propene observed for 2,3-dimethylbutane and the highest concentrations of ethylene in *n*-hexane. As for the laminar burning velocity, *n*-hexane/air laminar flame propagates fastest followed by 3-methylpentane/air and 2-methylpentane/air, while 2,3-dimethylbutane/air laminar flame propagates slowest. The *n*-hexane flame is easy to produce ethyl, but difficult to produce methyl, and has the largest ethylene concentration and smallest propene concentration, so it has the strongest reactivity and the highest laminar burning velocity. The 2,3-dimethylbutane flame is difficult to produce ethyl, easy to produce methyl, and has the lowest ethylene concentration and highest propene concentration, so it has the lowest reactivity and the slowest laminar burning velocity.

Author contributions

The authors confirm contribution to the paper as follows: study conception and design: Zhang J, Li S; data collection: Zhang J, Fang J, Zhang Q; analysis and interpretation of results: Zhang J, Li W; draft manuscript preparation: Zhang J, Lian T, Li W. All authors reviewed the results and approved the final version of the manuscript.

Data availability

All data generated or analyzed during this study are included in this published article.

Acknowledgments

This work was supported by the funding support from the National Natural Science Foundation of China (52206164), AECC Innovation Funds (ZZCX-2021-003), Science Center for Gas Turbine Project (P2022-B-II-017-001), and the Oceanic Interdisciplinary Program of Shanghai Jiao Tong University (SL2022ZD104).

Conflict of interest

The authors declare that they have no conflict of interest. Dr. Wei Li is the Editorial Board member of *Progress in Reaction Kinetics and Mechanism* who was blinded from reviewing or making decisions on the manuscript. The article was subject to the journal's standard procedures, with peer-review handled independently of this Editorial Board member and the research groups.

Supplementary information accompanies this paper at (https://www.maxapress.com/article/doi/10.48130/prkm-0024-0001)

Dates

Received 16 October 2024; Revised 26 November 2024; Accepted 2 December 2024; Published online 24 December 2024

References

1. Richards GA, McMillian MM, Gemmen RS, Rogers WA, Cully SR. 2001. Issues for low-emission, fuel-flexible power systems. *Progress in Energy and Combustion Science* 27:141–69
2. Blakey S, Rye L, Wilson CW. 2011. Aviation gas turbine alternative fuels: A review. *Proceedings of the Combustion Institute* 33:2863–85
3. Bayindirli C, Celik M. 2019. Investigation of combustion and emission characteristics of n-hexane and n-hexadecane additives in diesel fuel. *Journal of Mechanical Science and Technology* 33:1937–46
4. Çelīk M, Bayindirli C. 2020. Enhancement performance and exhaust emissions of rapeseed methyl ester by using n-hexadecane and n-hexane fuel additives. *Energy* 202:117643
5. Zhong A, Li X, Turányi T, Huang Z, Han D. 2022. Pyrolysis and oxidation of a light naphtha fuel and its surrogate blend. *Combustion and Flame* 240:111979
6. Li W, Wang GQ, Li YY, Li TY, Zhang Y, et al. 2018. Experimental and kinetic modeling investigation on pyrolysis and combustion of n-butane and i-butane at various pressures. *Combustion and Flame* 191:126–41
7. Li W, Zhang Y, Mei BW, Li YY, Cao CC, et al. 2019. Experimental and kinetic modeling study of n-propanol and i-propanol combustion: Flow reactor pyrolysis and laminar flame propagation. *Combustion and Flame* 207:171–85
8. Li W, Mei BW, Li YY, Eckart S, Krause H, et al. 2021. Insight into fuel isomeric effects on laminar flame propagation of pentanones. *Proceedings of the Combustion Institute* 38:2135–42
9. Zhang Y, Mei BW, Zhang XY, Ma SY, Li YY. 2021. Exploring fuel isomeric effects on laminar flame propagation of butylbenzenes at various pressures. *Proceedings of the Combustion Institute* 38:2419–29
10. Ribaucour M, Minetti R, Sochet LR, Curran HJ, Pitz WJ, Westbrook CK. 2000. Ignition of isomers of pentane: An experimental and kinetic modeling study. *Proceedings of the Combustion Institute* 28:1671–78
11. Silke EJ, Curran HJ, Simmie JM. 2005. The influence of fuel structure on combustion as demonstrated by the isomers of heptane: a rapid compression machine study. *Proceedings of the Combustion Institute* 30:2639–47
12. Zhang KW, Banyon C, Burke U, Kukkadapu G, Wagnon SW, et al. 2019. An experimental and kinetic modeling study of the oxidation of hexane isomers: Developing consistent reaction rate rules for alkanes. *Combustion and Flame* 206:123–37

13. Zhang Y, Zhang X, Cao C, Zou J, Li T, et al. 2021. Flow reactor pyrolysis of iso-butylbenzene and tert-butylbenzene at various pressures: Insight into fuel isomeric effects on pyrolysis chemistry of butylbenzenes. *Proceedings of the Combustion Institute* 38:1423–32
14. Lovell WG. 1948. Knocking characteristics of hydrocarbons. *Industrial & Engineering Chemistry* 40:2388–438
15. McEnally CS, Pfefferle LD. 2007. Improved sooting tendency measurements for aromatic hydrocarbons and their implications for naphthalene formation pathways. *Combustion and Flame* 148:210–22
16. Mével R, Chatelain K, Boettcher PA, Dayma G, Shepherd JE. 2014. Low temperature oxidation of n-hexane in a flow reactor. *Fuel* 126:282–93
17. Wang Z, Herbinet O, Cheng Z, Husson B, Fournet R, et al. 2014. Experimental investigation of the low temperature oxidation of the five isomers of hexane. *The Journal of Physical Chemistry A* 118:5573–94
18. Zhang KW, Banyon C, Togbe C, Dagaut P, Bugler J, Curran HJ. 2015. An experimental and kinetic modeling study of n-hexane oxidation. *Combustion and Flame* 162:4194–207
19. Yasunaga K, Yamada H, Oshita H, Hattori K, Hidaka Y, Curran H. 2017. Pyrolysis of n-pentane, n-hexane and n-heptane in a single pulse shock tube. *Combustion and Flame* 185:335–45
20. Kathrotia T, Oßwald P, Köhler M, Slavinskaya N, Riedel U. 2018. Experimental and mechanistic investigation of benzene formation during atmospheric pressure flow reactor oxidation of n-hexane, n-nonane, and n-dodecane below 1200 K. *Combustion and Flame* 194:426–38
21. Belhadj N, Lailliau M, Benoit R, Dagaut P. 2021. Experimental and kinetic modeling study of n-hexane oxidation. Detection of complex low-temperature products using high-resolution mass spectrometry. *Combustion and Flame* 233:111581
22. Burcat A, Olchanski E, Sokolinski C. 1996. Kinetics of hexane combustion in a shock tube. *Israel Journal of Chemistry* 36:313–20
23. Burcat A, Olchanski E, Sokolinski C. 1999. 2-Methyl-pentane ignition kinetics in a shock-tube. *Combustion Science and Technology* 147:1–37
24. Zhukov VP, Sechenov VA, Starikovskii AY. 2004. Ignition delay times in lean n-hexane-air mixture at high pressures. *Combustion and Flame* 136:257–59
25. Figueroa-Labastida M, Kashif TA, Farooq A. 2023. Dual-camera high-speed imaging of n-hexane oxidation in a high-pressure shock tube. *Combustion and Flame* 248:112586
26. Subburaj J, Kashif TA, Farooq A. 2023. Methane and n-hexane ignition in a newly developed diaphragmless shock tube. *Combustion and Flame* 253:112818
27. Davis SG, Law CK. 1998. Determination of and fuel structure effects on laminar flame speeds of C_1 to C_8 hydrocarbons. *Combustion Science and Technology* 140:427–49
28. Ji C, Dames E, Wang YL, Wang H, Egolfopoulos FN. 2010. Propagation and extinction of premixed C_5-C_{12} n-alkane flames. *Combustion and Flame* 157:277–87
29. Kelley AP, Smallbone AJ, Zhu DL, Law CK. 2011. Laminar flame speeds of C_5 to C_8 n-alkanes at elevated pressures: Experimental determination, fuel similarity, and stretch sensitivity. *Proceedings of the Combustion Institute* 33:963–70
30. Burluka AA, Gaughan RG, Griffiths JF, Mandilas C, Sheppard CGW, Woolley R. 2016. Turbulent burning rates of gasoline components, Part 1 - Effect of fuel structure of C_6 hydrocarbons. *Fuel* 167:347–56
31. Li X, Hu E, Lu X, Huang S, Huang Z. 2019. Experimental and kinetic study on laminar flame speeds of hexene isomers and n-hexane. *Fuel* 243:533–40
32. Konnov AA, Mohammad A, Kishore VR, Kim NI, Prathap C, Kumar S. 2018. A comprehensive review of measurements and data analysis of laminar burning velocities for various fuel + air mixtures. *Progress in Energy and Combustion Science* 68:197–267
33. Ranzi E, Frassoldati A, Grana R, Cuoci A, Faravelli T, et al. 2012. Hierarchical and comparative kinetic modeling of laminar flame speeds of hydrocarbon and oxygenated fuels. *Progress in Energy and Combustion Science* 38:468–501
34. Matras D, Villermaux J. 1973. Un réacteur continu parfaitement agité par jets gazeux pour l'étude cinétique de réactions chimiques rapides. *Chemical Engineering Science* 28:129–37
35. David R, Matras D. 1975. Règies de construction et d'extrapolation des réacteurs auto-agités par jets gazeux. *The Canadian Journal of Chemical Engineering* 53:297–300
36. Battin-Leclerc F, Herbinet O, Glaude PA, Fournet R, Zhou ZY, et al. 2010. Experimental confirmation of the low-temperature oxidation scheme of alkanes. *Angewandte Chemie-International Edition* 49:3169–72
37. Zhang XY, Li YY, Cao CC, Zou JB, Zhang Y, et al. 2019. New insights into propanal oxidation at low temperatures: An experimental and kinetic modeling study. *Proceedings of the Combustion Institute* 37:565–73
38. Wang ZD, Bian HT, Wang Y, Zhang LD, Li YY, et al. 2015. Investigation on primary decomposition of ethylcyclohexane at atmospheric pressure. *Proceedings of the Combustion Institute* 35:367–75
39. Mei BW, Zhang XY, Ma SY, Cui ML, Guo HW, et al. 2019. Experimental and kinetic modeling investigation on the laminar flame propagation of ammonia under oxygen enrichment and elevated pressure conditions. *Combustion and Flame* 210:236–46
40. Wang ZD, Zhao L, Wang Y, Bian HT, Zhang LD, et al. 2015. Kinetics of ethylcyclohexane pyrolysis and oxidation: An experimental and detailed kinetic modeling study. *Combustion and Flame* 162:2873–92
41. Sun WY, Yang B, Hansen N, Westbrook CK, Zhang F, et al. 2016. An experimental and kinetic modeling study on dimethyl carbonate (DMC) pyrolysis and combustion. *Combustion and Flame* 164:224–38
42. Wang GQ, Li YY, Yuan WH, Zhou ZBA, Wang Y, Wang ZZ. 2017. Investigation on laminar burning velocities of benzene, toluene and ethylbenzene up to 20 atm. *Combustion and Flame* 184:312–23
43. Bradley D, Gaskell PH, Gu XJ. 1996. Burning velocities, markstein lengths, and flame quenching for spherical methane-air flames: A computational study. *Combustion and Flame* 104:176–98
44. Burke MP, Chen Z, Ju YG, Dryer FL. 2009. Effect of cylindrical confinement on the determination of laminar flame speeds using outwardly propagating flames. *Combustion and Flame* 156:771–79
45. Kelley AP, Jomaas G, Law CK. 2009. Critical radius for sustained propagation of spark-ignited spherical flames. *Combustion and Flame* 156:1006–13
46. Zhang XY, Lailliau M, Cao CC, Li YY, Dagaut P, et al. 2019. Pyrolysis of butane-2, 3-dione from low to high pressures: Implications for methyl-related growth chemistry. *Combustion and Flame* 200:69–81
47. Peukert SL, Sivaramakrishnan R, Michael JV. 2015. High temperature rate constants for H/D + n-C_4H_{10} and i-C_4H_{10}. *Proceedings of the Combustion Institute* 35:171–79
48. Orme JP, Curran HJ, Simmie JM. 2006. Experimental and modeling study of methyl cyclohexane pyrolysis and oxidation. *The Journal of Physical Chemistry A* 110:114–31
49. Goos E, Hippler H, Hoyermann K, Jürges B. 2001. Reactions of methyl radicals with isobutane at temperatures between 800 and 950 Kelvin. *International Journal of Chemical Kinetics* 33:732–40
50. Badra J, Elwardany A, Farooq A. 2015. Shock tube measurements of the rate constants for seven large alkanes + OH. *Proceedings of the Combustion Institute* 35:189–96
51. CHEMKIN-PRO 15092. 2009. *Reaction Design*. San Diego
52. Miller JA, Klippenstein SJ. 2003. The recombination of propargyl radicals and other reactions on a C_6H_6 potential. *The Journal of Physical Chemistry A* 107:7783–99
53. Ji CS, Sarathy SM, Veloo PS, Westbrook CK, Egolfopoulos FN. 2012. Effects of fuel branching on the propagation of octane isomers flames. *Combustion and Flame* 159:1426–36